iScience

CellPress
OPEN ACCESS

Article

An ultrasensitive nanofiber-based assay for enzymatic hydrolysis and deep-sea microbial degradation of cellulose

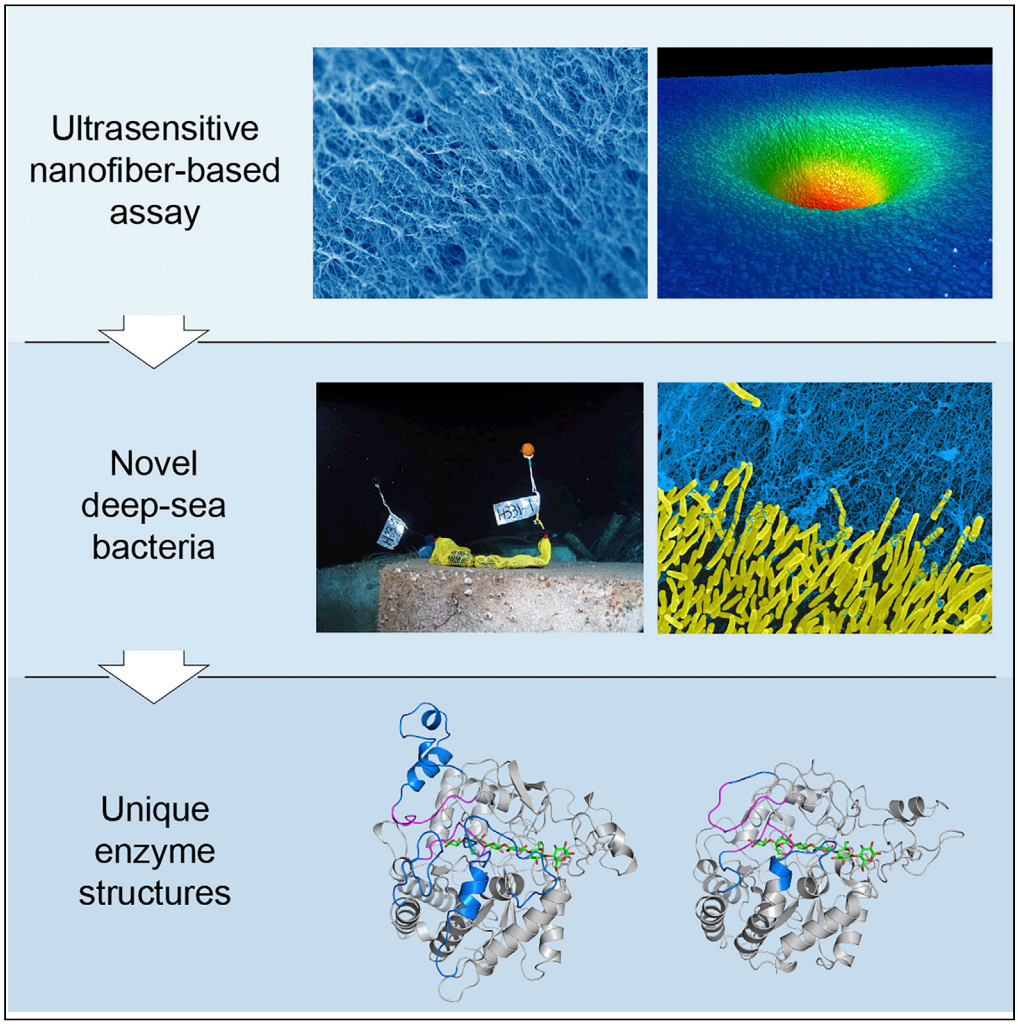

Mikiko Tsudome, Mikako Tachioka, Masayuki Miyazaki, Kohsuke Uchimura, Miwako Tsuda, Yoshihiro Takaki, Shigeru Deguchi

shigeru.deguchi@jamstec.go.jp

Highlights

Nanofiber-based method for quantifying enzymatic hydrolysis of cellulose at nanoscale

Identified previously unknown bacteria capable of degrading cellulose in deep sea

Molecular structures of cellulose hydrolysis are unique to a deep-sea bacterium

Significant portion of the cellulose from land eventually ends up in deep sea

Tsudome et al., iScience 25, 104732
August 19, 2022
https://doi.org/10.1016/j.isci.2022.104732

iScience

CellPress
OPEN ACCESS

Article

An ultrasensitive nanofiber-based assay for enzymatic hydrolysis and deep-sea microbial degradation of cellulose

Mikiko Tsudome,[1] Mikako Tachioka,[1] Masayuki Miyazaki,[2] Kohsuke Uchimura,[1,3] Miwako Tsuda,[2] Yoshihiro Takaki,[2] and Shigeru Deguchi[1,4,*]

SUMMARY

Substrates for enzymatic reactions, such as cellulose and chitin, are often insoluble in water. The enzymatic degradation of these abundant organic polymers plays a dominant role in the global carbon cycle and has tremendous technological importance in the production of bio-based chemicals. In addition, biodegradation of plastics is gaining wide attention. However, despite the significance, assaying these degradation reactions remains technically challenging owing to the low reaction rate, because only the surface of the substrate is accessible to the enzymes. We developed a nanofiber-based assay for the enzymatic hydrolysis of cellulose. This assay facilitated the quantification of the enzymatic hydrolysis of <1 ng crystalline cellulose. Utilization of the assay for the functional screening of cellulolytic microorganisms revealed an unprecedented genetic diversity underlying the production of deep-sea cellulase. This study reiterates that interdisciplinary efforts, such as from nanotechnology to microbiology, are critical for solving sustainability challenges.

INTRODUCTION

Cellulose, which is a linear and non-ionic polysaccharide comprising glucose connected via β-1-4 glycosidic linkages (Klemm et al., 2005), is the major component of plant cell walls and the most abundant organic polymer with an estimated annual production of ~100 billion dry tons (Percival Zhang et al., 2006). Hydrolysis of cellulose by microbial cellulases is the primary process for the turnover of photosynthetically fixed carbon in the global carbon cycle (Percival Zhang et al., 2006; Wilson, 2011; Cragg et al., 2015; Lynd et al., 2002). Microbial cellulases are also deemed crucial components for establishing biorefineries from this inexhaustible feedstock (Percival Zhang et al., 2006; Menon and Rao, 2012; Payne et al., 2015).

All cellulases cleave the β-1-4 glycosidic bonds in water-soluble substrates such as cellodextrins and carboxymethyl cellulose (CMC) and water-insoluble amorphous cellulose (Bayer et al., 1998). However, crystalline cellulose is resistant to enzymatic hydrolysis owing to extensive and highly ordered hydrogen bonding networks between the cellulose chains, whereas its hydrolysis usually requires the synergetic action of multiple enzymes. Glycoside hydrolases (GHs) that are classified as endoglucanases and exoglucanases (or cellobiohydrolases) play a primary role in generating short oligosaccharides (Payne et al., 2015; Hemsworth et al., 2016). Exoglucanases are known to be capable of breaking down crystalline regions of cellulose by detaching single cellulose chains from the crystal surface and guiding them into their long tunnel-shaped catalytic sites for hydrolysis (Beckham et al., 2014). Efficient hydrolysis is achieved with the assistance of oxidative enzymes such as copper-dependent lytic polysaccharide mono-oxygenases, which cleave the internal glycosidic bonds of crystalline cellulose and make it accessible for GHs (Beeson et al., 2015). The major soluble product of these enzymatic reactions is cellobiose, which is hydrolyzed to glucose by β-glucosidase. The degradation of the crystalline portion is the rate-limiting step in cellulose degradation; cellulolytic microorganisms have adapted their enzyme production mechanism so as to enable cooperative and efficient degradation. Some microorganisms produce cellulases as free enzymes which are often modular in nature and connected with carbohydrate-binding modules (CBMs) (Lynd et al., 2002; Payne et al., 2015), while some anaerobic microorganisms produce them as elaborate supra-molecular complexes called cellulosomes (Lynd et al., 2002; Bayer et al., 1998).

[1]Research Center for Bioscience and Nanoscience, Japan Agency for Marine-Earth Science and Technology (JAMSTEC), 2-15 Natsushima-cho, Yokosuka 237-0061, Japan

[2]SUGAR Program, JAMSTEC, 2-15 Natsushima-cho, Yokosuka 237-0061, Japan

[3]Present address: Bioengineering Lab. Co., Ltd., 657 Nagatake, Midori-ku, Sagamihara 252-0154, Japan

[4]Lead contact

*Correspondence: shigeru.deguchi@jamstec.go.jp

https://doi.org/10.1016/j.isci.2022.104732

For most enzymatic reactions, the quantitative assay of enzymatic hydrolysis of cellulose was usually performed by measuring the accumulation of end-products (Dashtban et al., 2010; Chang et al., 2021; Cruys-Bagger et al., 2012). However, existing methods were insensitive and time-consuming, primarily owing to the recalcitrance and water-insolubility of crystalline cellulose (Percival Zhang et al., 2006; Dashtban et al., 2010; Chang et al., 2021; Cruys-Bagger et al., 2012). These difficulties facilitated the introduction of unconventional techniques to study cellulase reactions. For example, high-speed atomic force microscopy (Ando, 2012) was successfully used to visualize cellulose hydrolysis by individual enzyme molecules; this revealed that the reaction was affected by the aggregation of the cellulase molecules on the cellulose surface (Igarashi et al., 2011; Igarashi, 2013) Quartz crystal microbalance with dissipation monitoring (QCM-D) was used to register the mass loss of cellulose films on hydrolysis (Ahola et al., 2008). It allowed the real-time observation of enzyme binding and hydrolysis kinetics, and revealed information about the morphological changes in the substrates. In the present study, we quantified the loss in cellulose volume on enzymatic hydrolysis using nanofibrous substrates, combined with inkjet patterning and three-dimensional (3D) laser profilometry. The novel technology, denoted as SPOT (Surface Pitting Observation Technology), facilitates ultrasensitive and quantitative assessment with potential high-throughput (multi-parallel) and diverse/flexible applications.

RESULTS

Surface pitting on nanofibrous cellulose matrix

To address the challenge of cellulose degradation detection owing to the low rate of cellulose hydrolysis, nanofibrous cellulose was prepared as previously described (Deguchi et al., 2007) to accelerate the enzymatic hydrolysis. When crystalline cellulose (Figure 1A; cellulose-I, 58.2% crystallinity) (Deguchi et al., 2007) and nanofibrous cellulose (Figure 1B; cellulose-II, 44.5% crystallinity) (Deguchi et al., 2007) were subjected to enzymatic hydrolysis using a mixture of fungal cellulases from *Trichoderma viride* (Winarni et al., 2013), the amount of glucose that was produced from nanofibrous cellulose after 30 min of reaction (1.4 mg/mL) was 3.5 times higher than that from the cellulose powder (0.4 mg/mL) (Figure S1). The difference could be ascribed to a significantly larger specific surface area of nanofibrous cellulose (220 m^2/g) than that of the cellulose powder (1.8 m^2/g) (Figure S1). The accessibility to the cellulose surface is a critical factor influencing the hydrolysis rate (Meng and Ragauskas, 2014). The difference in the crystallinity (Deguchi et al., 2007) is also substantial (~$3/4^{th}$) and should be a key factor (Hall et al., 2010). In addition, the difference in cellulose polymorphs could affect the hydrolysis rate, because the cellulose edge chains in cellulose II are less thermodynamically stable than those in cellulose I (Beckham et al., 2011). During the reaction, initially turbid dispersion containing fine particles made of nanofibrous cellulose was cleared in 2 h, whereas the dispersion containing the cellulose powder remained turbid even after 4 h of hydrolysis (Figures 1C–1D and Video S1). The observation shows that the hydrolysis of water-insoluble substrates such as cellulose can alternatively be assayed by following the loss of substrates.

In SPOT, this was realized by performing the reaction on the surface of nanofibrous cellulose matrices. When 18, 36, and 54 pL of a solution containing the cellulases (10 mg/mL) were inkjet-patterned on the flat surface of a wet porous matrix made of nanofibrous cellulose (Deguchi et al., 2007), the enzymes hydrolyzed the nanofibers as they diffused through the pores of the matrix and destroyed their 3D network, leading to the formation of pits on the surface (Figure 1E). The actual mass of the cellulases that were deposited was 0.18, 0.36, and 0.54 ng, respectively.

We used 3D optical profilometry to obtain a height map of the pitted surface in a non-destructive manner (Figure 1F). The space inside the pit remained dry, because the excess water released during the disruption of the 3D network was re-absorbed by the surrounding matrix. The pit formation was reproducible, because cross-sectional profiles that were obtained along the white lines on the map superimposed well on each other (Figure 1G). It is also evident that the pits became deeper with increasing amounts of deposited cellulases. These results suggest that surface pitting can potentially be used as a quantitative indicator to follow cellulose hydrolysis using an extremely small amount of enzyme.

Quantifying surface pitting to assay cellulase reaction

Measurements of pit formation kinetics revealed that the surface pitting was not only a quantitative indicator but also an ultrasensitive indicator to assay cellulase reaction. The pit grew after initiating the reaction by cellulase deposition and became deeper as a function of reaction time (Figures 2A and 2B, 3D height maps are available in Figure S2). The cross-sectional profile allows analysis of the 3D topographic features of the pit (illustrated by a thick red curve in Figure 2C); however, it does not provide information required to evaluate the progress of the reaction, such as the mass of hydrolyzed cellulose. Therefore, we measured the

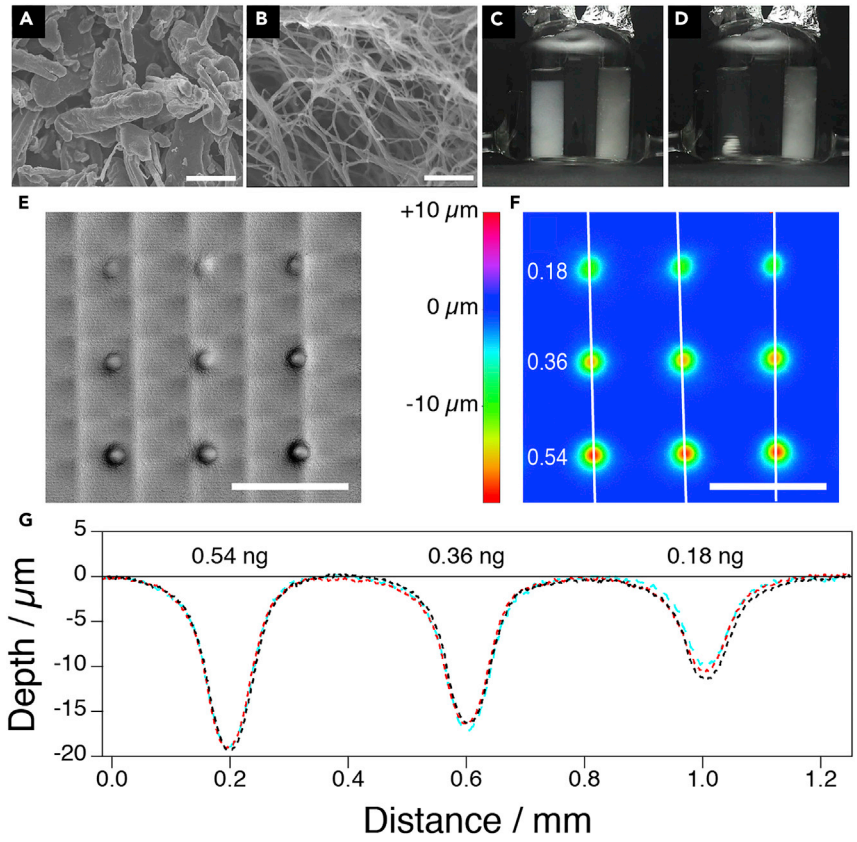

Figure 1. Surface pitting on nanofibrous cellulose matrix

Scanning electron microscopy images comparing the morphology of (A) untreated cellulose powder (scale bar: 5 μm) and (B) nanofibrous cellulose (scale bar: 500 nm) (taken from Deguchi et al., 2007). Photographs showing nanofibrous cellulose (left) and untreated cellulose powder (right) after enzymatic digestion for (C) 0 min and (D) 120 min in 0.1 M acetate buffer (pH 4.8) at 40°C (test tube diameter: 10 mm). A video of the hydrolysis process is available online (Video S1). Omnifocal microscopic image (E) and 3D height map (F) of pits formed on the surface of nanofibrous cellulose (0.03 g·cm^{-3} cellulose) containing 0.1 M acetate buffer (pH 4.8) after depositing 0.18, 0.36, and 0.54 ng of the cellulases. Scale bars represent 500 μm. Vertical lines in E are artifacts that were introduced when multiple images were computationally stitched to generate a panoramic image.

(G) A cross-sectional profile of the pits measured along the white lines in (F). Profiles were arbitrarily shifted horizontally to match the positions of the peaks.

volume of the pit (Figure 2D) and calculated the actual mass of hydrolyzed cellulose (illustrated by thick grey lines in Figure 2D) by multiplication with the fiber density of the matrix (0.03 g/cm^3).

The measured mass of hydrolyzed cellulose increased linearly with the reaction time up to 15 min, but the growth slowed down thereafter (Figure 2E). The initial hydrolysis rates, which were obtained from the slope of linear fits to the data points within 15 min, were between 60 and 180 pg·min^{-1} and proportional to the amount of deposited cellulases (Figure 2F). It should be noted that the actual amount of hydrolyzed cellulose might have been much smaller as only parts of the nanofibers required hydrolysis to separate them, sufficiently destroying the porous framework and pitting the surface.

Surface pitting as a selective indicator for the hydrolysis of crystalline cellulose

With a crystallinity index of 0.45 (Deguchi et al., 2007), nanofibrous cellulose is a blend of recalcitrant crystalline domains and easily hydrolyzable amorphous domains. Hydrolysis of the latter alone may also lead to pit formation. However, we found that a β-1-4 endoglucanase from *Bacillus agaradhaerens*, which hydrolyses CMC and amorphous cellulose but not crystalline cellulose (Hirasawa et al., 2006), showed near-zero hydrolytic activity against nanofibrous cellulose (Table S1), suggesting that surface pitting is a selective indicator for hydrolysis of crystalline cellulose.

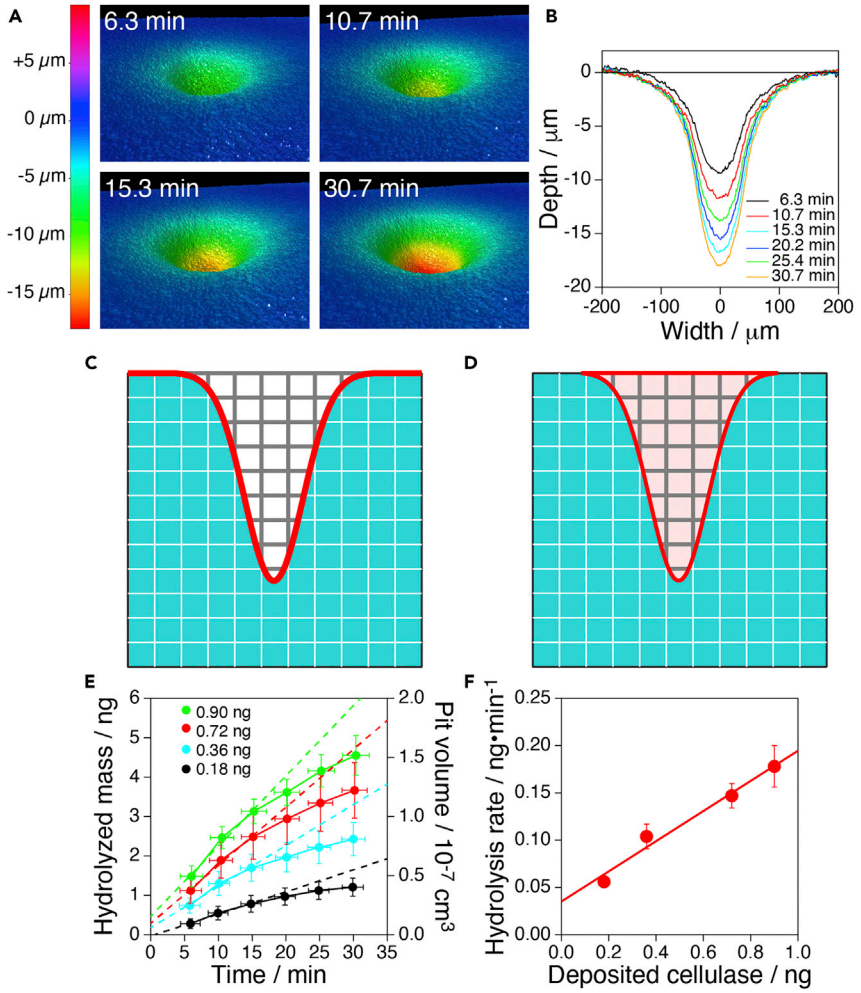

Figure 2. Quantifying pitting kinetics on nanofibrous cellulose matrix

(A) 3D topographic images of a pit formed on the surface of nanofibrous cellulose matrix (0.03 g·cm^{-3} cellulose) containing 0.1 M acetate buffer (pH 4.8) 6.3–30.7 min after depositing 0.90 ng cellulases.

(B) Cross-sectional profile of the pit as a function of reaction time. Schematic illustration for quantifying the cross-sectional profile (C) and volume (D) of each pit. White lines represent cellulose nanofibers and blue areas the buffered solution that filled up the cellulose matrix. The pit volume (pink area in D) allows calculating the mass of the hydrolyzed cellulose nanofibers (thick grey lines in D) by multiplying it with the fiber density.

(E) Change in the hydrolyzed mass of cellulose and the volume of the pit formed at 25°C after depositing 0.18 (black), 0.36 (blue), 0.72 (red), and 0.90 ng (green) cellulases. Data points represent the mean ± standard deviation (vertical bars) of at least five independent runs. Horizontal error bars represent the duration of scans to obtain 3D height maps (~5 min). Broken lines are linear fits to the first three data points.

(F) Relationship between the measured hydrolysis rate and amount of deposited cellulases.

Surface pitting for recognizing the microbial production of cellulase

Surface pitting can also be used to recognize the production of cellulases by microorganisms with high sensitivity. It was previously reported that various microorganisms (e.g., *Escherichia coli*, *Bacillus subtilis*, *Saccharomyces cerevisiae*, and several extremophiles) formed colonies when they were cultured on the surface of nanofibrous cellulose plates containing appropriate nutrients (Figure 3A, A 3D height map is available in Figure S3A) (Deguchi et al., 2007; Tsudome et al., 2009). However, when we cultured a model cellulase-producer *Saccharophagus degradans* 2–40^{T} (ATCC 43961) (Taylor et al., 2006; Jung et al., 2014), cellulases produced by the organism hydrolyzed nanofibrous cellulose and pit the plate surface (Figures 3B–3D, 3D height maps are available in Figures S3B–S3D). A small and shallow pit appeared after incubation for 24 h and grew with the incubation time (Figures 3E–3F).

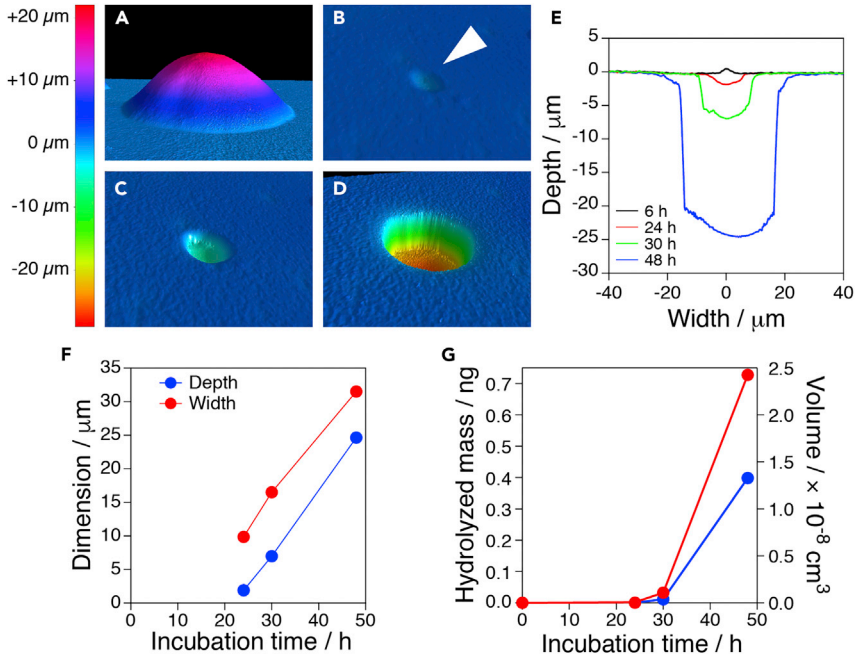

Figure 3. Recognizing microbial production of cellulases by surface pitting

(A) 3D topography of a colony of *Escherichia coli* formed on nanofibrous cellulose matrix containing Luria-Bertani medium after incubation at 37°C for 9 h. 3D topography of a pit formed by *S. degradans* on a nanofibrous cellulose matrix (0.03 $g \cdot cm^{-3}$ cellulose) after incubation at 25°C for (B) 24 h, (C) 30 h, and (D) 48 h.

(E) Cross-sectional profile of the pit over incubation time.

(F) Depth and width (full width at half depth) of the pit over incubation time. The linear relationship suggests the isotropic growth of the pit.

(G) The hydrolyzed mass of cellulose and volume of pits over incubation time. Red points represent the pit in (E), whereas blue points represent separate measurements to determine variation.

Second, the size of the pit the bacterium produced (Figure 3G) was an order of magnitude smaller than those obtained by depositing a solution of the cellulases (Figure 2E). In the case of the pit formed after incubation for 24 h (Figure 3B), the amount of hydrolyzed cellulose was 1.6 pg, which corresponds to $1/100^{th}$ the weight of a grain of cellulose (Figure S4). Because the specific gravity of cellulose is 1.48–1.63 $g \cdot cm^{-3}$ (Aulin et al., 2010), the volume of 1.6 pg monolithic cellulose is $\sim 1 \times 10^{-12}$ cm^3, which is too small to be detected by the present experimental set-up. Indeed, the low fiber density of the porous substrate (0.03 $g \cdot cm^{-3}$) facilitated the detection of cellulose hydrolysis because hydrolysis of a minute amount of cellulose led to a large volume change (Figure 2D).

Third, the microbial pitting did not slow down but rather accelerated with longer incubation times (Figure 3G); this could be attributed to the increase in the amount of enzymes with increased bacterial growth. Further incubation of *S. degradans* for 1 week led to the formation of millimeter-sized macroscopic pits (Figure S5A), thereby allowing facile recognition of microbial production of cellulases by visual inspection. Moreover, compared with a standard method for recognizing microbial cellulolytic activity toward crystalline cellulose (Hendricks et al., 1995), activity recognition by surface pitting took a significantly shorter time (Figure S5). Surface pitting was also a selective indicator for the microbial production of cellulases that hydrolyze crystalline cellulose (Figure S6).

Screening of cellulolytic bacteria from the deep sea

Culture-independent metagenomic approaches have been successfully used to mine cellulase genes and elucidate the diversity of microbial cellulases (Wilson, 2011; Li et al., 2009; Duan and Feng, 2010). For obtaining novel cellulases from natural environments, however, the metagenomic approach should be complemented by conventional culture-dependent methods (Duan and Feng, 2010). Culture-dependent screening of cellulolytic microorganisms takes full advantage of the ultrasensitivity of surface pitting for identifying cellulase activity. In selecting cellulolytic microorganisms out of an overwhelming majority of

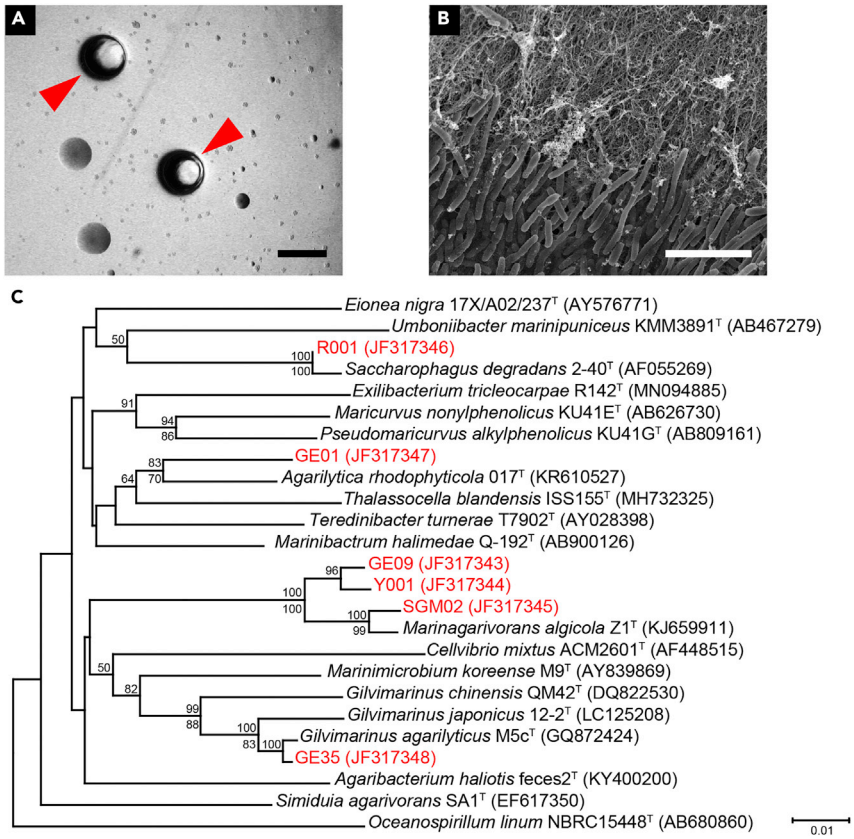

Figure 4. Isolation of cellulolytic bacteria from the deep sea

(A) Optical micrograph after incubation at 20°C for 15 d showing the surface of a nanofibrous cellulose plate during initial screening from Okinawa Trough. Cellulolytic bacteria formed pits (red triangles), easily separable from non-cellulolytic bacteria forming normal colonies of different sizes (scale bar: 1 mm).

(B) Scanning electron microscopy showing novel deep-sea bacteria (strain GE09; bottom) growing in a pit on a nanofibrous cellulose plate (0.01 g·cm^{-3} cellulose; top) after incubation at 20°C for 6 days (scale bar: 5 μm).

(C) Phylogeny of the deep-sea cellulolytic bacteria based on 16S rRNA gene sequence. Phylogenetic tree was constructed using the neighbor-joining method and numbers at nodes are bootstrap percentages ≥70% based on the neighbor-joining (higher nodes) and maximum-likelihood (lower nodes) methods. The bar represents 0.01 nucleotide substitutions per site. GenBank accession numbers are shown in parentheses.

non-cellulolytic ones in environmental samples (Wilson, 2011), ultrasensitive detection is crucial to recognize the microbial production of low concentrations of cellulases.

To demonstrate the performance, we deployed sterilized nanofibrous cellulose plates in the deep sea using research submersibles (Figure S7) and studied the cellulolytic activity of deep-sea bacteria that attached to the plate after recovery. From pits that were formed on the plate surface (Figure 4A), we successfully isolated six cellulolytic strains. The scanning electron microscope image in Figure 4B shows one of the isolates, strain GE09, grew and pit on the surface of a nanofibrous cellulose plate. The surface of the pit was covered with a dense mat of rod-shaped cells. Identification using 16S rRNA gene sequences (Weisburg et al., 1991) showed that the isolates were classified into the family *Cellvibrionaceae* within the class γ-Proteobacteria (Figure 4C). Strains GE09, Y001, and SGM02 exhibited 97%, 98%, and 99% homology, respectively, to *Marinagarivorans algicola* Z1^T, a marine degrader of agar and CMC (Guo et al., 2016). The isolates exhibited low homology (92%) to *Teredinibacter turnerae* T0971^T, which is a marine cellulolytic bacterium isolated from shipworms (Yang et al., 2009). Strain GE01 exhibited 96% homology to *Agarilytica rhodophyticola* 017^T, which has the ability to degrade agar but not cellulose (Ling et al., 2017). Strain R001 showed 99% identity to *S. degradans* 2–40^T (Weiner et al., 2008). Strain GE35 showed 98% identity to the marine cellulolytic bacterium *Gilvimarinus japonicus* 12-2^T (Kouzui et al., 2016). Strains GE09 and GE01 were likely novel bacterial species or genera.

The deep-sea isolates did not grow well in liquid culture media even though the pits expanded over millimeter or centimeter scales around where they were inoculated on the nanofibrous cellulose plates. The observations indicated that pit growth was not correlated with the quantitative growth of bacterial cell biomass, but simply represents the hydrolytic activities of the enzymes they produce. The GE09 strain consistently established large pits on cellulose plates and its cell/optical density at 600 nm could reach 0.1–0.3 in liquid media; therefore, we used GE09 for further analyses. We did not detect the cellulolytic activity of bacteria in a parallel screening attempt using a conventional method (agar plates with crystalline cellulose powder), suggesting that surface pitting on nanofibrous cellulose allowed isolating novel cellulolytic microorganisms unrecognized by the conventional method.

Insights into plant cell wall degradation by the deep-sea bacterium GE09

We determined the complete genome of one of the isolated bacterial species, strain GE09, as the statistical genome features shown in Table S2. Many extracellular polysaccharide-degrading enzymes were identified in its genome, potentially playing important roles to acquire nutrients and fixed carbon. A total of 79 coding sequences were predicted as targets for secretion and code at least one domain sequence assigned to the families in the carbohydrate-active enzymes database (CAZy database, http://www.cazy.org) (Lombard et al., 2014). Figure 5A shows its classification based on their target substrates in comparison with closely related marine γ-proteobacteria *T. turnerae* (Yang et al., 2009) and *S. degradans* (Weiner et al., 2008). Predicted enzymes targeting cellulose, hemicellulose (xylan and mannan), and pectin, which are the major components of plant cell walls, accounted for a remarkable proportion of secreted CAZymes in GE09 (Figure 5A, left). In contrast, there were only a few candidate genes of enzymes dedicated to marine polysaccharide degradation such as alginate and laminarin. Chitinase and agarase genes were not found in their genomes which agrees with our experimental observation that they could not grow on chitin and agar as sole carbon sources. These results indicate that GE09 specializes to degrade plant cell walls in analogy with the endosymbiont of shipworm, *T. turnerae*, rather than diversifying to degrade marine polysaccharides as is the case for the free-living bacterium *S. degradans*.

Characteristics of cellulases from the deep-sea bacterium GE09

The strain GE09 encoded more than ten genes of major cellulases in their genomes, whose catalytic domains were classified into GH family 5, 6, and 9 in the CAZy database as listed in Table S3. Many of them were predicted to have the type II secretion signal, which indicated that proteins were anchored to bacterial cellular membranes rather than secreted as free enzymes. The existence of several exo-type cellulases containing GH family 6 domains was noteworthy as they were necessary for degrading the crystalline part of cellulose. All genes of GH family 6 domain were classified into branches that were distinctly different from the majority of bacterial CBH genes in phylogenetic analysis (Figure 5B, branches indicated as GE09-a and GE09-b). As shown in one of the modeled structures of GH family 6 domains of GE09 (Figure 5B, right, top panel, Video S2), there were many sequence insertions (blue-colored regions) in the GE09 cellulase gene relative to the experimentally determined structure of bacterial CBH, *Thermobifida fusca* Cel6B (Sandgren et al., 2013) (Figure 5B, bottom right). Although its core structure and the loops adjacent to the active sites were structurally conserved, the inserted loop regions created more covered ligand binding sites, which would especially affect its catalytic activity, such as substrate uptake and processive degradation of insoluble crystalline substrates. Increased covered catalytic sites facilitate enzyme processivity by maintaining single-polysaccharide chains detached from the insoluble material, which might be an evolutionary conserved strategy for the degradation of recalcitrant polysaccharides (Uchiyama et al., 2020). The catalytically active status of two genes from GE09 (shown in branch GE09-b in the phylogenetic tree) was uncertain as they lacked essential catalytic residues.

Another characteristic feature of the cellulase genes from the deep-sea bacterium was their unique molecular architectures (Figure 5C). Instead of CBMs that are usually found in combination with catalytic domains of bacterial cellulases, the most found domain was polycystic kidney disease (PKD) in GH family 6 cellulase genes, and no CBMs could be solely judged by the genome sequencing results. In addition, there was an unknown sequence composed of ~250 amino acids at the C-terminus of a putative cellulase gene MARGE09_P3218 (Figure 5C, top), which commonly used databases such as BLAST, Pfam, and dbCAN (Zhang et al., 2018) failed to annotate. We found that it shared structural similarity with cellulose-induced protein I (CIP1), which is known as a protein of unknown function co-regulated by cellulases (Jacobson et al., 2013). There were completely unfamiliar modular architectures such as the sequence MARGE09_P1318 (Figure 5C, bottom) and the sequence MARGE09_P1043 that had peculiar characteristics in terms of their high-molecular weight (~3,400 amino acids, Table S3). These findings suggest that some remarkable changes occurred through the different combinations of accessory domains, not only in the sequences of catalytic core domains.

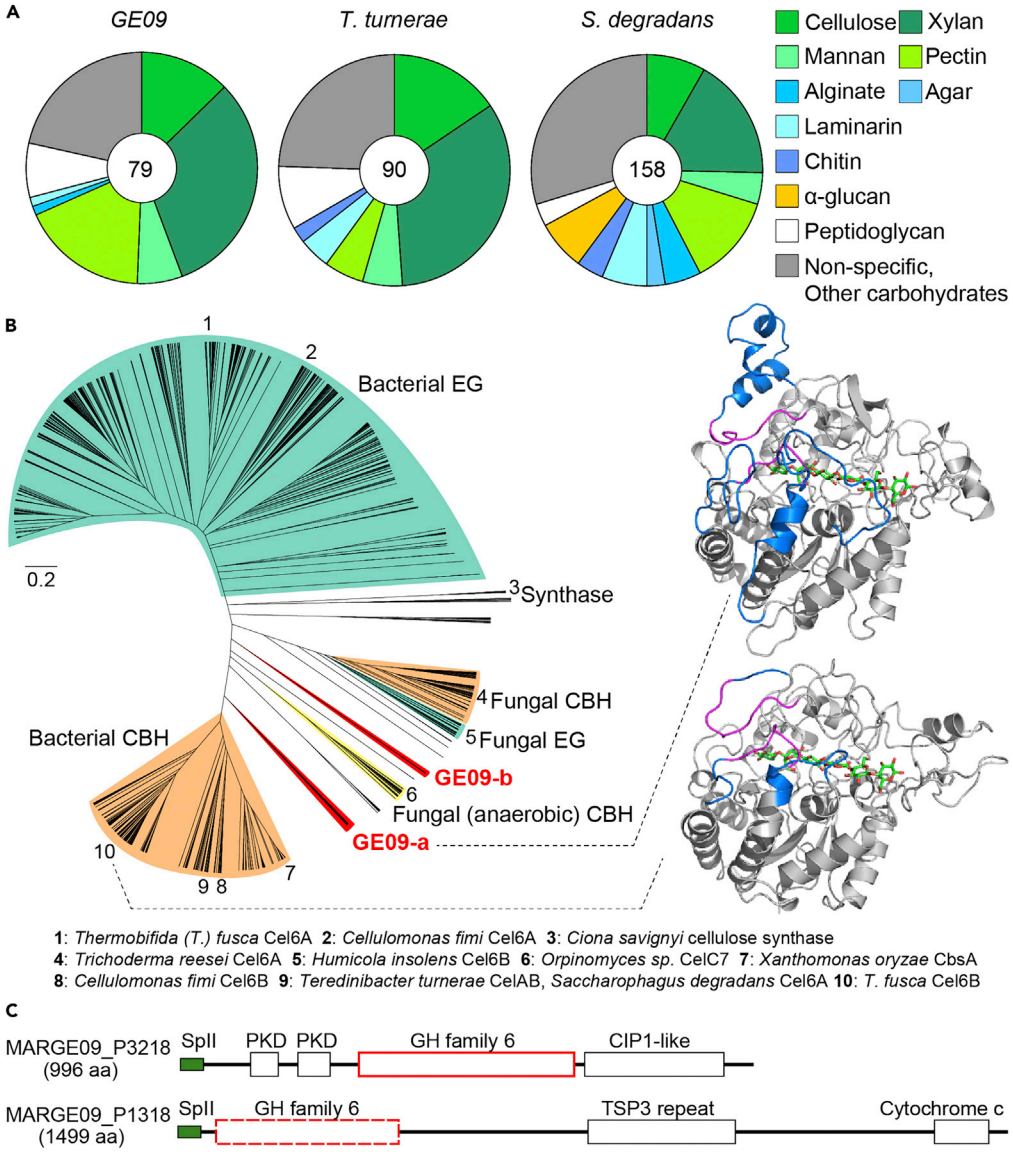

Figure 5. Predicted carbohydrate-active enzyme (CAZyme) genes from the deep-sea bacterium GE09 and the characteristics of its cellulases

(A) Predicted genes encoding CAZy domains with type I or II secretion signals in the genomes of GE09, *Teredinibacter turnerae*, and *Saccharophagus degradans*. The total number of sequences is shown in the center of each chart.

(B) Phylogenetic tree of the GH family 6 domain of all entries in the CAZy database and five sequences from GE09. Branches of GE09 sequences were indicated as branch GE09-a and GE09-b, colored in red. EG, endo-glucanase; CBH, cellobiohydrolase. A structure of the cellulase of GE09 (MARGE09_P1668) modeled using the online version of AlphaFold2, available via Colab (https://github.com/sokrypton/ColabFold), and the structure of the *T. fusca* Cel6B (-Sandgren et al., 2013) (Protein Data Bank accession code 4B4F), are shown on the right. Both models contain cellohexaoses at their ligand binding sites taken from *T. fusca* Cel6B (green). Loops adjacent to the binding sites and inserted loop regions were colored in magenta and blue, respectively.

(C) Previously undescribed modular structures of cellulases. GH family 6 domains shown with dotted line lack essential catalytic residues. SpII, type II secretion signal; PKD, polycystic kidney disease; CIP1, cellulose-induced protein I; TSP3, thrombospondin type 3.

DISCUSSION

Previously, mass loss of thin films of nanofibrous cellulose was measured by QCM-D to study the kinetics of their hydrolysis (Ahola et al., 2008). The method allowed real-time observation of enzyme binding and

hydrolysis kinetics, as well as giving information about morphological changes in the substrates. Our results complement this previous study by demonstrating that the volume loss can also be used for the analysis. Unlike QCM-D measurements, in which the mass loss is registered by a change in a resonant frequency of a quartz crystal, SPOT can estimate the actual weight of hydrolyzed cellulose. Furthermore, SPOT significantly extends the substrate-loss-based analysis by enabling a new realm of applications such as analysis using picoliter-quantities of a cellulase solution, detection of microbial production of cellulases that hydrolyze crystalline cellulose, and screening of cellulolytic microorganisms. SPOT could also be used to develop massively parallel analysis (Figures 1E and 1F).

Successful isolation of novel cellulolytic bacteria from the deep sea not only demonstrates the advantage of surface pitting for detecting microbial cellulase production but also suggests that cellulolytic bacteria may play a key ecological role in the unidentified carbon cycle and food web in the deep ocean (Glud et al., 2013) —even though cellulose is not photosynthetically produced *in situ* below 200 m owing to the lack of sunlight (Littler et al., 1985). With an annual production of 10^6–10^7 tons (Park and Kim, 2010), chitin used to be considered the most abundant organic polymer in the marine environment (Souza et al., 2011). Recent progress in the study of plastic pollution in the ocean, however, has revealed massive discharge of organic materials from land to the deep sea. It is estimated that more than 10^7 tons of plastic are discharged into the global ocean each year and 99% of it ends up in the deep sea (Kane et al., 2020). Given that the annual production of cellulose (10^{11} tons) (Percival Zhang et al., 2006) far outstrips that of plastic (10^8 tons) (Jehanno et al., 2022), it is likely that an enormous amount of cellulose of terrestrial origin settles in the deep sea and nourishes microbial ecosystems. Unique features that were predicted for cellulolytic enzymes from the isolated bacterium GE09, such as cell-membrane-associated cellulases with unknown domain structures, also suggest that the previously undetectable, and therefore undiscovered, genetic diversity in the deep sea is a promising pool for prospecting cellulolytic enzymes.

The high sensitivity of SPOT is attributable to the large specific surface area and porous structure of nanofibrous cellulose used as the reaction substrate. In principle, SPOT should be applicable in the study of enzymic hydrolysis of polymers that can be developed into porous nanofibrous matrices. Examples include polysaccharides such as chitin (Ding et al., 2012), proteins such as gelatin (Djabourov, 1988), and biodegradable synthetic polymers such as poly(L-lactic acid) (Yang et al., 2004). All these nanofibrous substrates are prepared by microphase separation in solutions. The range of application of SPOT could be further expanded if nanofibers prepared by other methods, such as electrospinning (Bhardwaj and Kundu, 2010), can be used as substrates.

Sustainability is the greatest challenge that our society is facing today. Exploiting enzymatic degradation of water-insoluble polymers is crucial to solving key sustainability challenges, such as the production of bio-based chemicals and the remediation of plastic pollution. The present study, which adopted a novel, highly sensitive, and relatively simple approach to quantify substrate loss that could be applied to other insoluble organic polymers, demonstrates that solving these challenges requires a truly interdisciplinary effort that encompasses diverse disciplines from nanotechnology to microbiology.

Limitations of the study

The hydrolyzability of cellulose depends on the crystalline parameters such as the degree of crystallinity and crystalline polymorph (Percival Zhang et al., 2006; Payne et al., 2015), as well as the surface area of the substrate. The crystalline structure of nanofibrous cellulose cannot be controlled in the present method of preparation; therefore, SPOT is not appropriate for investigating such effects. The major factor for the accelerated hydrolysis of nanofibrous cellulose should be elucidated. The use of substrates prepared using different methods could be a potential solution for overcoming this limitation.

Evaluation of the hydrolysis products could augment the analysis of the enzymatic reaction. However, the enzymatic degradation of crystalline polysaccharides is difficult to study, because insoluble substrates are not amenable to straightforward biochemical analysis and soluble intermediate products are degraded fast; therefore, they are difficult to detect. In SPOT, the analysis of the products is more difficult, especially, because of the small amount of hydrolysis. Therefore, our data do not directly conclude that surface pitting is the result of complete cellulose degradation; it is likely that the surface pitting occurred owing to the breakdown of nanocellulose into soluble or dispersible fragments.

STAR★METHODS

Detailed methods are provided in the online version of this paper and include the following:

- KEY RESOURCES TABLE
- RESOURCE AVAILABILITY
  - Lead contact
  - Materials availability
  - Data and code availability
- EXPERIMENTAL MODEL AND SUBJECT DETAILS
  - Culture of *E. coli*
  - Culture of *S. degradans*
  - Culture of *B. agaradhaerens*
- METHOD DETAILS
  - Preparation of nanofibrous cellulose
  - Brunauer-Emmett-Teller (BET) surface area
  - Enzymatic hydrolysis
  - Enzymatic surface pitting
  - Laser profilometry
  - Determination of pit volume
  - Screening of deep-sea cellulase producers
  - Sampling operation of deep-sea bacteria
  - Scanning electron microscopy
  - Sequencing and phylogenetic analysis of 16S rRNA genes
  - Genome sequencing of the strain GE09
  - Identification of carbohydrate-active enzymes (CAZymes)
  - Characterization of cellulase genes from the strain GE09

SUPPLEMENTAL INFORMATION

Supplemental information can be found online at https://doi.org/10.1016/j.isci.2022.104732.

ACKNOWLEDGMENTS

The authors received funding from the Japanese Society for the Promotion of Science, Grant-in-Aid for Scientific Research on Innovative Areas grant JP25120512 (SD, MT); Japanese Society for the Promotion of Science, Grant-in-Aid for Young Scientists (B) grant JP25850127 (MT); grant JP26850226 (KU); Japanese Society for the Promotion of Science, Grant-in-Aid for Young Scientists grant JP19K15956 (MTa); Shimadzu Science Foundation (SD); Japan Prize Foundation (MT); and Kyokuto Pharmaceutical Industrial Co., Ltd. (SD, MT, KU).

Yoshihiro Fujiwara, Satoshi Konishi, Sumihiro Koyama, Kaoru Kubokawa, Tetsuya Miwa, and Yuichi Nogi assisted with the collection of the samples. We thank Tohru Hamatani for kindly supplying us with Meicelase, Yasushi Hori for assistance in inkjet patterning, Katsuyuki Uematsu, and Akihiro Tame for technical assistance in SEM observations, and Ryusuke Nabata for measurements of the specific surface area. We are grateful to Koki Horikoshi, Susumu Ito, Kaoru Tsujii, Tohru Kobayashi, Kiyohiko Igarashi and Taku Uchiyama for stimulating discussion. Kyokuto Pharmaceutical Industrial Co., Ltd. is also acknowledged for placing the 3D laser profiler at our disposal.

AUTHOR CONTRIBUTIONS

Conceptualization: S.D.; Methodology: M.T., M.Ta., M.M., K.U., M.Tsuda; Investigation: M.T., M.Ta., M.M., K.U., M.Tsuda., S.D.; Visualization: M.T., M.Ta., S.D.; Formal analysis: M.Ta., Y.T., S.D.; Supervision: S.D.; Writing—original draft: M.Ta., Y.T., S.D.; Writing—review & editing: S.D.

DECLARATION OF INTERESTS

JAMSTEC has patents relating to the production and uses of the nanofibrous cellulose plate, of which SD and MT are named inventors. SD and MT have received research support and may profit from the sale of the nanofibrous cellulose plate, which has been developed by Kyokuto Pharmaceutical Industrial Co., Ltd., Japan, through a joint research agreement with JAMSTEC. All other authors declare no competing interests.

Received: March 28, 2022
Revised: May 10, 2022
Accepted: July 2, 2022
Published: July 25, 2022

SUPPORTING CITATIONS

The following references appear in the Supplemental information: Smith (1977).

REFERENCES

Ahola, S., Turon, X., Österberg, M., Laine, J., and Rojas, O.J. (2008). Enzymatic hydrolysis of native cellulose nanofibrils and other cellulose model films: effect of surface structure. Langmuir *24*, 11592–11599.

Ando, T. (2012). High-speed atomic force microscopy coming of age. Nanotechnology *23*, 062001.

Aulin, C., Gällstedt, M., and Lindström, T. (2010). Oxygen and oil barrier properties of microfibrillated cellulose films and coatings. Cellulose *17*, 559–574.

Bayer, E.A., Chanzy, H., Lamed, R., and Shoham, Y. (1998). Cellulose, cellulases and cellulosomes. Curr. Opin. Struct. Biol. *8*, 548–557.

Beckham, G.T., Matthews, J.F., Peters, B., Bomble, Y.J., Himmel, M.E., and Crowley, M.F. (2011). Molecular-level origins of biomass recalcitrance: decrystallization free energies for four common cellulose polymorphs. J. Phys. Chem. B *115*, 4118–4127.

Beckham, G.T., Ståhlberg, J., Knott, B.C., Himmel, M.E., Crowley, M.F., Sandgren, M., Sørlie, M., and Payne, C.M. (2014). Towards a molecular-level theory of carbohydrate processivity in glycoside hydrolases. Curr. Opin. Biotechnol. *27*, 96–106.

Beeson, W.T., Vu, V.V., Span, E.A., Phillips, C.M., and Marletta, M.A. (2015). Cellulose degradation by polysaccharide monooxygenases. Annu. Rev. Biochem. *84*, 923–946.

Bhardwaj, N., and Kundu, S.C. (2010). Electrospinning: a fascinating fiber fabrication technique. Biotechnol. Adv. *28*, 325–347.

Bolger, A.M., Lohse, M., and Usadel, B. (2014). Trimmomatic: a flexible trimmer for Illumina sequence data. Bioinformatics *30*, 2114–2120.

Chang, H., Wohlschlager, L., Csarman, F., Ruff, A., Schuhmann, W., Scheiblbrandner, S., and Ludwig, R. (2021). Real-time measurement of cellobiose and glucose formation during enzymatic biomass hydrolysis. Anal. Chem. *93*, 7732–7738.

Cragg, S.M., Beckham, G.T., Bruce, N.C., Bugg, T.D.H., Distel, D.L., Dupree, P., Etxabe, A.G., Goodell, B.S., Jellison, J., McGeehan, J.E., et al. (2015). Lignocellulose degradation mechanisms across the tree of life. Curr. Opin. Chem. Biol. *29*, 108–119.

Cruys-Bagger, N., Ren, G., Tatsumi, H., Baumann, M.J., Spodsberg, N., Andersen, H.D., Gorton, L., Borch, K., and Westh, P. (2012). An amperometric enzyme biosensor for real-time measurements of cellobiohydrolase activity on insoluble cellulose. Biotechnol. Bioeng. *109*, 3199–3204.

Dashtban, M., Maki, M., Leung, K.T., Mao, C., and Qin, W. (2010). Cellulase activities in biomass conversion: measurement methods and comparison. Crit. Rev. Biotechnol. *30*, 302–309.

Deguchi, S., Tsudome, M., Shen, Y., Konishi, S., Tsujii, K., Ito, S., and Horikoshi, K. (2007). Preparation and characterisation of nanofibrous cellulose plate as a new solid support for microbial culture. Soft Matter *3*, 1170–1175.

Ding, B., Cai, J., Huang, J., Zhang, L., Chen, Y., Shi, X., Du, Y., and Kuga, S. (2012). Facile preparation of robust and biocompatible chitin aerogels. J. Mater. Chem. *22*, 5801.

Djabourov, M. (1988). Architecture of gelatin gels. Contemp. Phys. *29*, 273–297.

Duan, C.J., and Feng, J.X. (2010). Mining metagenomes for novel cellulase genes. Biotechnol. Lett. *32*, 1765–1775.

El-Gebali, S., Mistry, J., Bateman, A., Eddy, S.R., Luciani, A., Potter, S.C., Qureshi, M., Richardson, L.J., Salazar, G.A., Smart, A., et al. (2019). The Pfam protein families database in 2019. Nucleic Acids Res. *47*, D427–D432.

Glud, R.N., Wenzhöfer, F., Middelboe, M., Oguri, K., Turnewitsch, R., Canfield, D.E., and Kitazato, H. (2013). High rates of microbial carbon turnover in sediments in the deepest oceanic trench on Earth. Nat. Geosci. *6*, 284–288.

Guo, L.Y., Li, D.Q., Sang, J., Chen, G.J., and Du, Z.J. (2016). *Marinagarivorans algicola* gen nov, sp nov, isolated from marine algae. Int. J. Syst. Evol. Microbiol. *66*, 1593–1599.

Hall, M., Bansal, P., Lee, J.H., Realff, M.J., and Bommarius, A.S. (2010). Cellulose crystallinity—a key predictor of the enzymatic hydrolysis rate. FEBS J. *277*, 1571–1582.

Hemsworth, G.R., Déjean, G., Davies, G.J., and Brumer, H. (2016). Learning from microbial strategies for polysaccharide degradation. Biochem. Soc. Trans. *44*, 94–108.

Hendricks, C.W., Doyle, J.D., and Hugley, B. (1995). A new solid medium for enumerating cellulose-utilizing bacteria in soil. Appl. Environ. Microbiol. *61*, 2016–2019.

Hirasawa, K., Uchimura, K., Kashiwa, M., Grant, W.D., Ito, S., Kobayashi, T., and Horikoshi, K. (2006). Salt-activated endoglucanase of a strain of alkaliphilic *Bacillus agaradhaerens*. Antonie Leeuwenhoek *89*, 211–219.

Hyatt, D., LoCascio, P.F., Hauser, L.J., and Uberbacher, E.C. (2012). Gene and translation initiation site prediction in metagenomic sequences. Bioinformatics *28*, 2223–2230.

Igarashi, K. (2013). Cellulases: cooperative biomass breakdown. Nat. Chem. Biol. *9*, 350–351.

Igarashi, K., Uchihashi, T., Koivula, A., Wada, M., Kimura, S., Okamoto, T., Penttilä, M., Ando, T., and Samejima, M. (2011). Traffic jams reduce hydrolytic efficiency of cellulase on cellulose surface. Science *333*, 1279–1282.

Ito, S., Kobayashi, T., Hatada, Y., and Horikoshi, K. (2005). Enzymes in modern detergents. In Microbial Enzymes and Biotransformations, J.L. Barredo, ed. (Humana Press), pp. 151–161.

Jacobson, F., Karkehabadi, S., Hansson, H., Goedegebuur, F., Wallace, L., Mitchinson, C., Piens, K., Stals, I., and Sandgren, M. (2013). The crystal structure of the core domain of a cellulose induced protein (Cip1) from *Hypocrea jecorina*, at 1.5 Å resolution. PLoS One *8*, e70562.

Jehanno, C., Alty, J.W., Roosen, M., De Meester, S., Dove, A.P., Chen, E.Y.-X., Leibfarth, F.A., and Sardon, H. (2022). Critical advances and future opportunities in upcycling commodity polymers. Nature *603*, 803–814.

Jin, H., Nishiyama, Y., Wada, M., and Kuga, S. (2004). Nanofibrillar cellulose aerogels. Colloids Surf. A Physicochem. Eng. Asp. *240*, 63–67.

Jumper, J., Evans, R., Pritzel, A., Green, T., Figurnov, M., Ronneberger, O., Tunyasuvunakool, K., Bates, R., Žídek, A., Potapenko, A., et al. (2021). Highly accurate protein structure prediction with AlphaFold. Nature *596*, 583–589.

Juncker, A.S., Willenbrock, H., von Heijne, G., Brunak, S., Nielsen, H., and Krogh, A. (2003). Prediction of lipoprotein signal peptides in Gram-negative bacteria. Protein Sci. *12*, 1652–1662.

Jung, Y.H., Kim, H.K., Song, D.S., Choi, I.G., Yang, T.H., Lee, H.J., Seung, D., and Kim, K.H. (2014). Feasibility test of utilizing *Saccharophagus degradans* 2-40^{T} as the source of crude enzyme for the saccharification of lignocellulose. Bioproc. Biosyst. Eng. *37*, 707–710.

Kalvari, I., Argasinska, J., Quinones-Olvera, N., Nawrocki, E.P., Rivas, E., Eddy, S.R., Bateman, A., Finn, R.D., and Petrov, A.I. (2018). Rfam 13.0: shifting to a genome-centric resource for non-coding RNA families. Nucleic Acids Res. *46*, D335–D342.

Kane, I.A., Clare, M.A., Miramontes, E., Wogelius, R., Rothwell, J.J., Garreau, P., and Pohl, F. (2020).

Seafloor microplastic hotspots controlled by deep-sea circulation. Science *368*, 1140–1145.

Katoh, K., Rozewicki, J., and Yamada, K.D. (2019). MAFFT online service: multiple sequence alignment, interactive sequence choice and visualization. Briefings Bioinf. *20*, 1160–1166.

Kelley, L.A., Mezulis, S., Yates, C.M., Wass, M.N., and Sternberg, M.J.E. (2015). The Phyre2 web portal for protein modeling, prediction and analysis. Nat. Protoc. *10*, 845–858.

Klemm, D., Heublein, B., Fink, H.P., and Bohn, A. (2005). Cellulose: fascinating biopolymer and sustainable raw material. Angew. Chem., Int. Ed. Engl. *44*, 3358–3393.

Kouzui, H., Tokikawa, K., Satomi, M., Negoro, T., Shimabukuro, K., and Fujii, K. (2016). *Gilvimarinus japonicus* sp nov, a cellulolytic and agarolytic marine bacterium isolated from coastal debris. Int. J. Syst. Evol. Microbiol. *66*, 5417–5423.

Kumar, S., Stecher, G., Li, M., Knyaz, C., and Tamura, K. (2018). MEGA X: molecular evolutionary genetics analysis across computing platforms. Mol. Biol. Evol. *35*, 1547–1549.

Larkin, M.A., Blackshields, G., Brown, N.P., Chenna, R., McGettigan, P.A., McWilliam, H., Valentin, F., Wallace, I.M., Wilm, A., Lopez, R., et al. (2007). Clustal W and clustal X version 2.0. Bioinformatics *23*, 2947–2948.

Leggett, R.M., Clavijo, B.J., Clissold, L., Clark, M.D., and Caccamo, M. (2014). NextClip: an analysis and read preparation tool for Nextera Long Mate Pair libraries. Bioinformatics *30*, 566–568.

Li, L.L., McCorkle, S.R., Monchy, S., Taghavi, S., and van der Lelie, D. (2009). Bioprospecting metagenomes: glycosyl hydrolases for converting biomass. Biotechnol. Biofuels *2*, 10.

Ling, S.K., Xia, J., Liu, Y., Chen, G.J., and Du, Z.J. (2017). *Agarilytica rhodophyticola* gen. nov., sp. nov., isolated from *Gracilaria blodgettii*. Int. J. Syst. Evol. Microbiol. *67*, 3778–3783.

Littler, M.M., Littler, D.S., Blair, S.M., and Norris, J.N. (1985). Deepest known plant life discovered on an uncharted seamount. Science *227*, 57–59.

Lombard, V., Golaconda Ramulu, H., Drula, E., Coutinho, P.M., and Henrissat, B. (2014). The carbohydrate-active enzymes database (CAZy) in 2013. Nucleic Acids Res. *42*, D490–D495.

Lowe, T.M., and Chan, P.P. (2016). TRNAscan-SE on-line: integrating search and context for analysis of transfer RNA genes. Nucleic Acids Res. *44*, W54–W57.

Luo, R., Liu, B., Xie, Y., Li, Z., Huang, W., Yuan, J., He, G., Chen, Y., Pan, Q., Liu, Y., et al. (2015). Erratum: SOAPdenovo2: an empirically improved memory-efficient short-read de novo assembler. GigaScience *4*, 30.

Lynd, L.R., Weimer, P.J., van Zyl, W.H., and Pretorius, I.S. (2002). Microbial cellulose utilization: fundamentals and biotechnology. Microbiol. Mol. Biol. Rev. *66*, 506–577.

Meng, X., and Ragauskas, A.J. (2014). Recent advances in understanding the role of cellulose accessibility in enzymatic hydrolysis of lignocellulosic substrates. Curr. Opin. Biotechnol. *27*, 150–158.

Menon, V., and Rao, M. (2012). Trends in bioconversion of lignocellulose: biofuels, platform chemicals & biorefinery concept. Prog. Energy Combust. Sci. *38*, 522–550.

Mirdita, M., Ovchinnikov, S., and Steinegger, M. (2021). ColabFold - making protein folding accessible to all. Preprint at bioRxiv. https://doi.org/10.1101/2021.08.15.456425.

Moore, A.D., Held, A., Terrapon, N., Weiner, J., and Bornberg-Bauer, E. (2014). DoMosaics: software for domain arrangement visualization and domain-centric analysis of proteins. Bioinformatics *30*, 282–283.

Park, B.K., and Kim, M.M. (2010). Applications of chitin and its derivatives in biological medicine. Int. J. Mol. Sci. *11*, 5152–5164.

Payne, C.M., Knott, B.C., Mayes, H.B., Hansson, H., Himmel, M.E., Sandgren, M., Ståhlberg, J., and Beckham, G.T. (2015). Fungal cellulases. Chem. Rev. *115*, 1308–1448.

Percival Zhang, Y.H., Himmel, M.E., and Mielenz, J.R. (2006). Outlook for cellulase improvement: screening and selection strategies. Biotechnol. Adv. *24*, 452–481.

Pryszcz, L.P., and Gabaldón, T. (2016). Redundans: an assembly pipeline for highly heterozygous genomes. Nucleic Acids Res. *44*, e113.

Saitou, N., and Nei, M. (1987). The neighbor-joining method: a new method for reconstructing phylogenetic trees. Mol. Biol. Evol. *4*, 406–425.

Sandgren, M., Wu, M., Karkehabadi, S., Mitchinson, C., Kelemen, B.R., Larenas, E.A., Ståhlberg, J., and Hansson, H. (2013). The structure of a bacterial cellobiohydrolase: the catalytic core of the *Thermobifida fusca* family GH6 cellobiohydrolase Cel6B. J. Mol. Biol. *425*, 622–635.

Smith, R.E. (1977). Rapid tube test for detecting fungal cellulase production. Appl. Environ. Microbiol. *33*, 980–981.

Souza, C.P., Almeida, B.C., Colwell, R.R., and Rivera, I.N.G. (2011). The importance of chitin in the marine environment. Mar. Biotechnol. *13*, 823–830.

Tamura, K., and Nei, M. (1993). Estimation of the number of nucleotide substitutions in the control region of mitochondrial DNA in humans and chimpanzees. Mol. Biol. Evol. *10*, 512–526.

Taylor, L.E., Henrissat, B., Coutinho, P.M., Ekborg, N.A., Hutcheson, S.W., and Weiner, R.M. (2006). Complete cellulase system in the marine bacterium *Saccharophagus degradans* strain 2–40^{T}. J. Bacteriol. *188*, 3849–3861.

Teather, R.M., and Wood, P.J. (1982). Use of Congo red-polysaccharide interactions in enumeration and characterization of cellulolytic bacteria from the bovine rumen. Appl. Environ. Microbiol. *43*, 777–780.

Tsudome, M., Deguchi, S., Tsujii, K., Ito, S., and Horikoshi, K. (2009). Versatile solidified nanofibrous cellulose-containing media for growth of extremophiles. Appl. Environ. Microbiol. *75*, 4616–4619.

Uchiyama, T., Uchihashi, T., Nakamura, A., Watanabe, H., Kaneko, S., Samejima, M., and Igarashi, K. (2020). Convergent evolution of processivity in bacterial and fungal cellulases. Proc. Natl. Acad. Sci. USA *117*, 19896–19903.

Honorato, R.V. (2016). CAZy-parser a way to extract information from the carbohydrate-Active enZYmes Database. J. Open Source Softw. *1*, 53.

Waterhouse, A., Bertoni, M., Bienert, S., Studer, G., Tauriello, G., Gumienny, R., Heer, F.T., de Beer, T.A.P., Rempfer, C., Bordoli, L., et al. (2018). SWISS-MODEL: homology modelling of protein structures and complexes. Nucleic Acids Res. *46*, W296–W303.

Weiner, R.M., Taylor, L.E., Henrissat, B., Hauser, L., Land, M., Coutinho, P.M., Rancurel, C., Saunders, E.H., Longmire, A.G., Zhang, H., et al. (2008). Complete genome sequence of the complex carbohydrate-degrading marine bacterium, *Saccharophagus degradans* strain 2–40^{T}. PLoS Genet. *4*, e1000087.

Weisburg, W.G., Barns, S.M., Pelletier, D.A., and Lane, D.J. (1991). 16S ribosomal DNA amplification for phylogenetic study. J. Bacteriol. *173*, 697–703.

Wilson, D.B. (2011). Microbial diversity of cellulose hydrolysis. Curr. Opin. Microbiol. *14*, 259–263.

Winarni, I., Oikawa, C., Yamada, T., Igarashi, K., Koda, K., and Uraki, Y. (2013). Improvement of enzymatic saccharification of unbleached cedar pulp with amphipathic lignin derivatives. Bioresources *8*, 2195–2208.

Yang, F., Murugan, R., Ramakrishna, S., Wang, X., Ma, Y.X., and Wang, S. (2004). Fabrication of nano-structured porous PLLA scaffold intended for nerve tissue engineering. Biomaterials *25*, 1891–1900.

Yang, J.C., Madupu, R., Durkin, A.S., Ekborg, N.A., Pedamallu, C.S., Hostetler, J.B., Radune, D., Toms, B.S., Henrissat, B., Coutinho, P.M., et al. (2009). The complete genome of *Teredinibacter turnerae* T7901: an intracellular endosymbiont of marine wood-boring bivalves (shipworms). PLoS One *4*, e6085.

Zhang, H., Yohe, T., Huang, L., Entwistle, S., Wu, P., Yang, Z., Busk, P.K., Xu, Y., and Yin, Y. (2018). dbCAN2: a meta server for automated carbohydrate-active enzyme annotation. Nucleic Acids Res. *46*, W95–W101.

STAR★METHODS

KEY RESOURCES TABLE

REAGENT or RESOURCE	SOURCE	IDENTIFIER
Bacterial and virus strains		
Escherichia coli W3110		ATCC 27325
Saccharophagus degradans 2–40^T		ATCC 43961
Bacillus agaradhaerens DSM8721^T	Hirasawa et al. (2006)	DSM 8721
Strain GE09	This study	DSM 113420
Chemicals, peptides, and recombinant proteins		
Microcrystalline cellulose	Merck	102331;CAS 9004-34-6
Meicelase (mixture of cellulases from *Trichoderma viride*)	Meiji Seika	N/A
β-1-4 Endoglucanase from *Bacillus agaradhaerens*	Hirasawa et al. (2006)	N/A
Critical commercial assays		
Glucose CII-Test Wako	Wako Pure Chemical	N/A
Deposited data		
16S rRNA sequences of strains GE09, Y001, SGM02, R001, GE01, and GE35	This study	JF317343–JF317348
Complete genome sequence of GE09	This study	AP023086
Software and algorithms		
Scanning Probe Image Processor (SPIP)	Image Metrology	https://www.imagemet.com
dbCAN2 v8	Zhang et al. (2018)	https://bcb.unl.edu/dbCAN2/
ColabFold	Mirdita et al. (2021)	https://github.com/sokrypton/ColabFold
Other		
3D laser scanning microscope, VK-9700 Generation II	Keyence	N/A
Inkjet patterning device, LaboJet-500Bio	Microjet Corporation	

RESOURCE AVAILABILITY

Lead contact

Further information and requests for resources should be directed to and will be fulfilled by the lead contact, Shigeru Deguchi (shigeru.deguchi@jamstec.go.jp).

Materials availability

All materials generated in this study are available from the lead contact without restriction.

Data and code availability

- The 16S rRNA gene sequence data of strains GE09, Y001, SGM02, R001, GE01, and GE35 and the complete genome sequence of GE09 have been submitted to the DDBJ/EMBL/GenBank DNA databases. The accession numbers are listed in the Key resources table.
- This paper does not report original code.
- Any additional information required to reanalyze the data reported in this paper is available from the lead contact upon request.

EXPERIMENTAL MODEL AND SUBJECT DETAILS

Culture of *E. coli*

E. coli W3110 (ATCC 27325) was cultured in LB broth at 37°C until absorbance at 600 nm (A_{600}) reached 1–1.5. The cultures were diluted with 0.9 wt % physiological saline to 1×10^4 cells mL^{-1}. The diluted culture

(100 μL) was spread onto the nanofibrous cellulose plate containing LB broth and incubated at 37°C for 9 h. 3D topographical image of a colony was obtained using a 3D laser scanning microscope (VK-9700 Generation II; Keyence, Osaka, Japan).

Culture of *S. degradans*

S. degradans 2–40^T (ATCC 43961) was cultured in marine broth (Difco 2216) supplemented with cellobiose (0.1 wt %) at 30°C for 3 d. The culture was diluted 10^6 times with artificial seawater (ASW, Marine Art SF-1; Senju Pharmaceutical, Osaka, Japan), spread on nanofibrous cellulose plates containing ASW plus ammonium sulphate (1 mM) and trace minerals (Solution A from *Teredinibacter* medium, ATCC medium no. 1983), and incubated at 30°C. A control experiment was performed on a gellan-gum plate containing the same medium and a fine powder of crystalline cellulose (cellulose microcrystalline for thin layer chromatography; Merck).

Culture of *B. agaradhaerens*

B. agaradhaerens DSM8721^T was cultured in alkaline nutrient medium containing (per liter) 10 g polypeptone S, 2.5 g fish extract, 5 g sodium glutamate, 5 g carboxymethyl cellulose (CMC), 1 g yeast extract, 0.015 g K_2HPO_4, 0.02 g $MgSO_4 \cdot 7H_2O$, 0.01 g $CaCl_2 \cdot 2H_2O$, and 5 g Na_2CO_3 (sterilized separately) at 30°C for 3 d (Hirasawa et al., 2006). The culture was diluted 10^6 times with alkaline nutrient medium, spread on nanofibrous cellulose plates containing half-strength alkaline nutrient medium without CMC, and incubated at 30°C. An optical image of the culture was taken with a flat-bed scanner (MP990; Canon).

Endoglucanase production of *B. agaradhaerens* was confirmed using Congo red staining (Teather and Wood, 1982). *B. agaradhaerens* was inoculated at the center of a nanofibrous cellulose plate containing alkaline nutrient medium without CMC and incubated at 30°C for 2 d. After growth of the organism, soft agar (0.8 wt % Agarose X; Wako Pure Chemical) containing 0.1 M glycine-NaOH buffer (pH 9) supplemented with 0.25 wt % CMC and 0.1 M NaCl was overlaid on top of the plate. The plate was incubated at 30°C for 2 h, and 10 mL water containing 0.1 wt % Congo red was placed on the plate surface. The plate was incubated for 10 min, and the excess Congo red solution was washed out with 1 M NaCl.

METHOD DETAILS

Preparation of nanofibrous cellulose

Nanofibrous cellulose plates were prepared according to the literature (Deguchi et al., 2007; Tsudome et al., 2009). Briefly, cellulose (microcrystalline cellulose for thin-layer chromatography; Merck, Darmstadt, Germany) was dissolved in a hot saturated solution of $Ca(SCN)_2$ in water at a concentration of 0.03 or 0.01 $g \cdot cm^{-3}$. The solution was allowed to solidify at 25°C overnight, during which the porous network of nanofibrous crystalline cellulose was spontaneously formed. $Ca(SCN)_2$ was removed from the solidified plates by washing them with methanol and water. The nano-porous structured gel (Figure 1B (Deguchi et al., 2007)) plates saturated with water were sealed and stored at 4°C until use.

Brunauer-Emmett-Teller (BET) surface area

Nanofibrous cellulose was subjected to solvent exchange with ethanol and *t*-butyl alcohol, followed by lyophilization (Jin et al., 2004). The sample was further treated in a vacuum at 120°C overnight to remove all the adsorbed species. Nitrogen adsorption measurements were performed at 77 K on a Tristar II 3020 (Micromeritics Instrument, Norcross, GA, USA). The BET analysis was performed for relative vapor pressure between 0.05 and 0.35.

Enzymatic hydrolysis

A plate of nanofibrous cellulose was crushed into fine particles and sieved (nominal aperture, 500 μm). The fine particles of nanofibrous cellulose and as-received cellulose powder were dispersed in 0.1 M acetate buffer (pH 4.8) at a concentration of 5 mg/mL and heated to 40°C with stirring. Hydrolysis was initiated by adding cellulases from *Trichoderma viride* (Meicelase; Meiji Seika, Tokyo, Japan) to the mixtures at a concentration of 1 mg/mL. Aliquots (100 μL) were taken at appropriate time intervals and boiled to terminate the reaction, and the concentration of glucose was assayed using a mutarotase-glucose oxidase kit (Glucose CII-Test Wako; Wako Pure Chemical, Osaka, Japan).

Purification and activity assay of β-1-4 endoglucanase from *Bacillus agaradhaerens* were performed in accordance with the published literature (Hirasawa et al., 2006). Relative hydrolytic activity toward nanofibrous cellulose was measured in 0.1 M glycine-NaOH buffer (pH 9.0) with 0.2 M NaCl. A plate of nanofibrous cellulose was crushed into fine particles and dispersed in the buffer at the concentration of 10 mg/mL. The reaction was allowed to proceed at 40°C overnight, and the concentration of accumulated reducing sugars was measured by 3,5-dinitrosalicylic acid (DNS) method (Ito et al., 2005).

Enzymatic surface pitting

Following the solvent exchange to 0.1 M acetate buffer (pH 4.8), the disc-shaped plates (~9 cm in diameter, ~5 mm thick) were cut into square pieces (1~3 cm across) and used as substrate for enzymatic pitting. A solution containing 10 mg/mL cellulases from *T. viride* (Meicelase; Meiji Seika, Tokyo, Japan) was deposited onto a flat surface of nanofibrous cellulose plate using an inkjet patterning device (LaboJet-500Bio; Microjet, Shiojiri, Japan) equipped with an IJHBS-10 inkjet head. The instrument was adjusted to deposit 9 pL cellulase solution per shot. The amount of deposited solution was controlled by repeatedly depositing the solution in the same place. Reactions were allowed to proceed at 25°C.

Laser profilometry

Pits on the surface of nanofibrous cellulose matrices were quantified using a VK-9700 Generation II (Keyence, Osaka, Japan), which is a confocal laser scanning microscope working in reflection mode. The surface of an object was laterally scanned using a laser (λ = 408 nm), and the intensity of reflected light from the surface, *I*, was measured by a photomultiplier. A field of view was divided to 1,024 × 768 pixels. Measurements were repeated while scanning the object in the depth (*z*) direction to obtain a stack of images, of which each pixel was associated with *z* and *I*. A focal position of a pixel was given at *z* where the strongest *I* was recorded. A 3D height map was generated by locating focal positions of all pixels in an image.

A 50× objective (N.A. 0.95, field of view: 270 μm × 202 μm) was used except for the observation of a *B. agaradhaerens* colony (Figures S6A–S6B), for which a 20× objective (N.A. 0.46, field of view: 675 μm × 506 μm) was used. Imaging was performed using the panorama-mode; multiple images were collected and computationally joined together to give an image covering an area larger than a single field of view. A humidifying chamber was used during measurements to minimize the evaporation of water from the wet nanofibrous cellulose matrices.

Determination of pit volume

Pit volume was determined from the 3D height map using Scanning Probe Image Processor (Image Metrology, Hørsholm, Denmark). The histogram in Figure S8 shows the distribution of depth data in height maps after applying polynomial plane correction (flattening). The roughness, root mean square deviation (Rq) of average amplitude in the height direction, was 0.2–0.4 μm. These surface areas were excluded from the calculation to eliminate the errors due to surface irregularities. Threshold was set to −1 μm, and depth data below the threshold were integrated (indicated by grey shades in the histograms) and multiplied by the pixel dimension (0.7 μm × 0.7 μm for 20× objective, 0.3 μm × 0.3 μm for a 50× objective). The threshold was set to −0.5 μm for the microbial pit by *S. degradans*.

Screening of deep-sea cellulase producers

Nanofibrous cellulose plates containing pure water were autoclaved at 121°C for 20 min. The plates were then transferred to a polystyrene Petri dish, and the lid and body were glued. A small gap was left between them so that water could go in and out of the dish, whereas the cellulose plate could not escape from the dish. Sampling operations were performed by exposing nanofibrous cellulose to deep-sea water (at the depth between 141 and 654 m) using the unmanned remotely operate vehicle Hyper-Dolphin or the manned submersible Shinkai 6500. Detailed sampling conditions are described in the next section. Upon recovery, the cellulose plates were immediately put in a sterile bag, sealed, and kept at 4°C until use.

The recovered plates were crushed into fine particles and dispersed in ASW. The dispersions were spread on fresh cellulose plates containing low nutrient media. ASW supplemented with 1 mM ammonium sulphate was used as the basal medium. Trace minerals (Solution A from *Teredinibacter* medium), vitamins (vitamin solution from heterotrophic medium H3P; DSM medium no. 428), and/or 0.005 wt % bonito extract (Wako Pure Chemical) were added in some cases. The plates were incubated at 15 or 20°C, and the plate

surface was inspected visually for the formation of pits. In the screening attempt off Noma Misaki (NT04-08_leg1), the recovered sample was also spread on agar plates containing cellulose powder; however, no cellulolytic activity of bacterial colonies was recognized on the plates.

When pits were formed on the surface of cellulose plates, microorganisms in the pits were picked up with toothpicks, dispersed in ASW, and then spread on fresh cellulose plates. In this way, we isolated six cellulolytic strains from Noma Misaki (strains GE01, GE09 and GE35), Kinko Bay (strains Y001 and R001), and Nankai Trough (strain SGM02). Strain GE09 colonized on the basal medium at 15°C. Strains GE01, Y001, R001, and SGM02 colonized on the basal medium supplemented with solution A and vitamin solution at 20°C. Strain GE35 colonized at 20°C on the basal medium amended with solution A, vitamin solution, and bonito extract.

Sampling operation of deep-sea bacteria

In situ sampling was performed using the unmanned ROV Hyper Dolphin off Noma Misaki at the depth of 225 m near sperm whale carcasses (dive nos. 328 and 332 during cruise NT04-08_leg1 (July 2004); dive no. 453 during cruise NT05-12 (July 2005); 31.3467°N, 129.9867°E). A plastic mesh bag containing the nanofibrous cellulose plates in Petri dishes was left at the sampling locations for 1 d or 1 year and recovered. In the sampling operations at Kinko Bay at the depth of 204 m (dive no. 381 during cruise NT05-01_leg2 (January 2005); 31.6617°N, 130.77330°E), the plates were left for 1 h.

In another sampling attempt off Noma Misaki at the depth of 223–227 m near sperm whale carcasses (dive no. 888 during cruise NT08-17_leg2 (August 2008); 31.3467°N, 129.9867°E), a mesh bag containing cellulose plates in culture dishes was fixed to the exterior of the submersible and exposed to deep-sea water during the survey for 2 h. A similar method was also used in a sampling operation using the manned submersible Shinkai 6500 at the Nankai Trough (dive no. 882 during cruise YK05-08_leg1 (June 2005); 34.0733°N, 137.7883°E) during a survey at the depth between 596 and 654 m for 6 h, and a sampling operation using the unmanned ROV Hyper Dolphin at the Okinawa Trough during a survey at the depth between 141 and 214 m for 2.5 h (dive no. 1061 during cruise NT09-17_leg1 (October 2009); 25.4468°N, 125.7390°E).

Scanning electron microscopy

Strain GE09 was incubated on nanofibrous cellulose plates at 20°C until visible pits (~1 mm in diameter) were formed; the pits were cut out with a sharp knife. The microbial cells were fixed in 2.5 wt % glutaraldehyde for 1 h, washed with 0.1 M phosphate buffered saline (PBS) for 15 min, fixed in 1 wt % OsO_4 for 1 h, and washed in 0.1 M PBS for 15 min. The specimens were subjected to solvent exchange with ethanol and *t*-butyl alcohol, followed by lyophilization. The lyophilized specimens were coated with osmium and examined on a JSM-6700F scanning electron microscope (JEOL, Tokyo, Japan).

Sequencing and phylogenetic analysis of 16S rRNA genes

The 16S rRNA gene was amplified through PCR using a DNA thermal cycler (model 9600; Perkin Elmer, Waltham, MA, USA), using the domain bacteria-specific primer 27f (5′ -AGAGTTTGATCCTGGCTCAG-3′) and the universal primer 1492R (5′ -GGTTACCTTGTTACGACTT-3′). The PCR product was sequenced using a DYEnamic ET Dye terminator and a MegaBACE 1000 DNA sequencer (GE Healthcare & Bio-Sciences, Uppsala, Sweden). Multiple alignments were performed using the CLUSTAL X program (Larkin et al., 2007) and a distance matrix tree was constructed based on the neighbor-joining (Saitou and Nei, 1987) and maximum-likelihood (Tamura and Nei, 1993) methods in MEGA X v10.2.4 (Kumar et al., 2018) The topology of the phylogenetic tree was evaluated by performing bootstrap analysis with 1,000 replicates. The available 16S rRNA sequences of the type strains in the family *Cellvibrionaceae* were used to construct the tree with *Oceanospirillum linum* NBRC 15448^T (GenBank: AB680860) as the outgroup.

Genome sequencing of the strain GE09

The strain GE09 was grown in liquid culture containing ASW, 1 mM ammonium sulphate, trace minerals (Solution A from *Teredinibacter* medium), and 1 wt % cellobiose for 7 d at 20°C and collected by centrifugation. Total genomic DNA was extracted using the NucleoSpin Tissue kit (Macherey-Nagel, Düren, Germany).

Illumina paired-end library from the extracted GE09 DNA was constructed with KAPA library prep kit (KAPA Biosystems, Wilmington, MA, USA) and mate-paired library was prepared from DNA fragments with an average insert length of 3 kb using Nextera Mate Pair Library Preparation Kit (Illumina, San Diego, CA, USA), according to the manufacturer's instructions. Both libraries were sequenced on an Illumina MiSeq platform with 300 bp paired-end sequences. Raw reads were processed using Trimmomatic v0.36 (Bolger et al., 2014) to trim the remaining adaptor and low-quality sequences. The linker sequence in mate-paired reads were removed using NextClip v1.3.1 (Leggett et al., 2014). The processed paired-end reads were assembled using CLC Genomic Workbench v11 (Qiagen, Hilden, Germany) with the parameter settings: k-mer value of 64 bp, bubble size of 500 bp, and map read back to the contigs with length fraction of 0.8 and similarity fraction of 0.8. The assembled contigs and the mate-paired reads were used as input into Redundans pipeline v0.14a (Pryszcz and Gabaldón, 2016), which merges redundant contigs and then scaffolds the resulting contigs. Finally, all gap regions within scaffolds were completely filled by GapCloser v1.12 (Luo et al., 2015) using the paired-end and mate-paired reads.

Protein coding genes in the GE09 genome were predicted using Prodigal v2.6.3 (Hyatt et al., 2012). Blast searches against the NCBI–nr and KEGG GENES databases were further performed to determine the coding sequences (CDSs). Their functional annotations were manually assigned based on the KEGG Orthology database. The prediction of genes for rRNA, tRNA, and other non-coding RNAs was performed with Barrnap v0.9 (https://github.com/tseemann/barrnap), tRNAscan-SE v1.3.1 (Lowe and Chan, 2016), and Rfam v13.0 (Kalvari et al., 2018), respectively.

Identification of carbohydrate-active enzymes (CAZymes)

The CAZyme genes were predicted in the genomes of GE09, *T. turnerae* T0971 (Genbank: NC_012997) (Yang et al., 2009), and *S. degradans* 2–40 (Genbank: NC_007912) (Weiner et al., 2008) using dbCAN2 v8 (Zhang et al., 2018). Its annotations were only adopted when at least two of the three tools yielded positive outputs. The signal peptides were predicted using LipoP v1.0 (Juncker et al., 2003). Secreted proteins, which were predicted to contain either type I or II secretion signal peptides, were 79, 90, and 158 sequences in GE09, *T. turnerae*, and *S. degradans*, respectively, and manually grouped according to their substrate specificities. Substrate specificities were predicted based on the CAZy family or subfamily classifications and manually completed by reference to annotations in *T. turnerae* (Yang et al., 2009) and *S. degradans* (Taylor et al., 2006; Weiner et al., 2008) as well as Blast searches against the NCBI database (https://blast.ncbi.nlm.nih.gov). The CAZy families were sorted as follows: cellulose, GH 5, 6, 9, 44, 45, AA 10; xylan, GH 2, 3, 8, 10, 11, 12, 27, 30, 31, 35, 39, 43, 51, 62, 67, 74, 115, CE 1, 3, 15; mannan, GH 2, 5, 26; pectin, GH 28, 105, PL 1, 3, 10, 11, CE 8, 12; alginate, PL 6, 7, 14, 17, 18; agar, GH 16, 50, 86; laminarin, GH 16, 30; chitin, GH18, 20; α-glucan (amylose and pullulan), GH 13, 15, 97; peptidoglycan, GH 23, 53, 73, 103, GT 51.

Characterization of cellulase genes from the strain GE09

To identify putative cellulase genes, translated protein sequences were scanned using dbCAN and Pfam (El-Gebali et al., 2019) databases and annotated using BLAST. The genes containing GH family 6 domains were further analyzed by structural modeling using the Phyre2 server (Kelley et al., 2015) and SWISS-MODEL (Waterhouse et al., 2018). The structural model in Figure 4 and Video S2 was prepared using the online version of AlphaFold2 (Jumper et al., 2021), available via Colab (https://github.com/sokrypton/ColabFold) (Mirdita et al., 2021). The phylogenetic tree of GH family 6 proteins was constructed as follows. All entries of GH family 6 proteins in CAZy database were downloaded by CAZy-parser (Honorato, 2016) and GH family domain regions were extracted by DoMosaics (Moore et al., 2014). Alignment of the total 1,827 sequences was then performed by MAFFT with E-NS-2 method (Katoh et al., 2019).